Synthesis and Characterization of Graphene Oxide-Cellulose Based Aerogels

Ho Khanh Ha Le[a,b], Lam Tuong Vy Nguyen[a,b], T Bich Ngoc Phung[a,b], Quen K[a,b], Yuta Nishina[c], Ky Phuong Ha Huynh[a,b], Truong Son Nguyen[a,b], Ngoc Do Quyen Chau[a,b,*]

[a]Ho Chi Minh City University of Technology (HCMUT), 268 Ly Thuong Kiet Street, District 10, Ho Chi Minh City, Vietnam
[b]Vietnam National University Ho Chi Minh City, Linh Trung Ward, Thu Duc District, Ho Chi Minh City, Vietnam
[c]Research Core for Interdisciplinary Sciences, Okayama University, 3-1-1 Tsushima-Naka, Kita-ku, Okayama, Japan
 cndquyen@hcmut.edu.vn

Two sources of cellulose used to fabricate graphene oxide-cellulose based aerogels were cellulose nanocrystals (CNC) and rice straw. Up to now, aerogels obtained from graphene oxide and cellulose in rice straw remain rare. In this report, aerogel materials show a strong ability that can be used in water treatment by adhering to a simple, green procedure. Scanning electron microscopy (SEM), Fourier-transform infrared spectroscopy (FT-IR), thermal gravimetric analysis (TGA), nitrogen physisorption isotherm were used to examine the shape, features, and physico-chemical properties of these aerogels. The aerogels exhibited high porosity (97.14-98.53 %) and low density (0.0197-0.0385 g/cm^3). In adsorption experiments, they showed a great capability in adsorption of Cu^{2+} (98.73-123.2 mg/g), of various oil types (up to 28.11 g/g) and of methylene blue (MB) (up to 96.23 %).

1. Introduction

Cellulose-based aerogels have been extensively studied over the last decades since the materials are biomass-derived, abundant, and renewable (Long et al., 2018). Graphene oxide (GO) owing a large surface area, a huge number of oxygenated groups on its surface, a high mechanical property, etc. has been considered to create a hybrid composites GO/cellulose with tunable properties that can be suitable for environmental applications. The mechanical properties of the obtained composite were better than that of neat cellulose aerogel (Zhang et al., 2012). The method to fabricate nanocomposite of GO/cellulose aerogels using NaOH/polyethylene glycol was reported (Wan et al., 2016). Another example that benefited from the strong interaction of hydroxyl groups in cellulose and carboxylic acid groups in GO was revealed by the development of a green synthesis of GO/microcrystalline cellulose composites (Wei et al., 2017). The hybrid aerogels showed an excellent adsorption ability toward MB. An ultralight carbon aerogel was successfully fabricated from hydroxypropyl methyl cellulose and GO (Jiang et al., 2020). The structure showed an extraordinary resilience and exceptional sensitivity. The group of Yao prepared the GO/nanocellulose aerogels for adsorption of MB and tetracycline (Wang et al., 2021). The adsorption ability of these composites was attributed to electrostatic and π-π interactions. Among these GO/cellulose composites, the aerogels that were fabricated under green process from GO and agricultural wastes has not been developed yet. By combining cellulose nanofibers obtained from the petioles of the nipa palm tree with GO, the group of Nguyen could fabricate the light and porous aerogels toward the adsorption of MB (Nguyen et al., 2022). Herein the methods to fabricate the aerogels from GO, polyvinyl alcohol (PVA) and CNC was reported. This green, facile method was then applied to create for the first time aerogels from GO, PVA and rice straw fiber as rice straw is a popular agricultural waste (Low et al., 2017). The characterizations, the adsorption capabilities of these two types of aerogels were investigated.

2. Experiments and methods

2.1 Materials

Rice straw was collected from Long An province, Vietnam, sanitized, and dried. An aqueous dispersion of GO was obtained following the modified Hummer method (Morimoto et al., 2016) and received from the group of Nishina. CNC was obtained from microcrystalline cellulose following the acid hydrolysis PVA was purchased from Shanghai Zhanyun Chemical Com, Ltd. Sodium hydroxide, hydrogen peroxide and hydrochloric acid were obtained from Xilong Scientific Co., Ltd. Motor oil 10W30 was purchased from Asian Honda Motor Co., Ltd. Soybean oil was obtained from a local supermarket. MB hydrate and Methyltrimethoxysilane (MTMS) were obtained from Sigma. Cu^{2+} was derived from copper (II) nitrate trihydrate obtained from Xilong Scientific Co., Ltd.

2.2 Pre-treatment of rice straw

Before pre-treatment, the straw was dried to eliminate excess moisture and blended into powder. Pre-treatment targets to detach lignin from cellulose. The solution of NaOH 1 M was used with the ratio of 10 g straw to 320 mL NaOH. The mixture was heated to 90 °C while stirring for 2 h. After that, the solution was filtered and neutralized (pH 7) using distilled water. The final residue was raw cellulose. It was bleached using the solution of H_2O_2 30 % with the ratio of 10 g cellulose to 14 mL H_2O_2 in pH 12 (via NaOH adjustment). Bleaching step lasted for 2 h with stirring at 90 °C. After that, the mixture was filtered, neutralized (pH 7) with distilled water and dried. The residue collected was utilized for preparing aerogels.

2.3 Fabrication of aerogel

Pre-treated rice straw fibre/CNC was dispersed in water, GO and PVA were added. The solution was stirred at 70 °C until a good dispersion was observed. The mixture was sonicated for 15 mins before stirring for 2 h. The final solution was moulded and kept frozen for a day. The frozen samples were freeze dried for 48 h to fabricate the aerogels. The first one, namely A1, was fabricated from aqueous GO, CNC, and PVA. The second one, namely A2, was fabricated by replacing CNC with pre-treated rice straw fibre.

2.4 Characterization methods

Brunauer-Emmett-Teller (BET) and Barrett Joyner Halenda (BJH) techniques were utilized to analyze the surface areas and pore size distribution of aerogel samples. The BET specific surface area was determined by Micromeritics Tristar 3030. SEM were carried out on the FE-SEM S-4800, Hitachi. FT-IR spectra were collected in the InfraRed Bruker Tensor 37. TGA was run on the Mettler Toledo TGA/DSC3 + LF.
The density of the aerogels was determined by using Eq(1):

$$\rho_{aerogels} = \frac{m_{aerogels}}{V_{aerogels}} \tag{1}$$

in which m (g) is the mass of aerogels, V (cm^3) is the volume of aerogels.
The porosity of aerogels was calculated by using Eq(2):

$$P(\%) = \left(1 - \frac{\rho}{\rho_{mixture}}\right).100 \tag{2}$$

in which ρ (g/cm^3) is the density of aerogels, $\rho_{mixture}$ (g/cm^3) is the average density of aerogel mixture and calculated by Eq(3):

$$\frac{1}{\rho_{mixture}} = \frac{W_{cellulose}}{\rho_{cellulose}} + \frac{W_{GO}}{\rho_{GO}} + \frac{W_{PVA}}{\rho_{PVA}} \tag{3}$$

where $W_{cellulose}$, W_{GO} and W_{PVA} is the mass component of cellulose, GO and PVA in mixture. $\rho_{cellulose}$, ρ_{GO} and ρ_{PVA} is the density of cellulose, GO and PVA (g/cm^3).

2.5 Studies of adsorption

2.5.1 Adsorption of methylene blue

The following procedure was used to determine the dye adsorption capacity of aerogels: samples were dispersed into a 100 mL dye solution of different initial concentrations. The Spectro UV-VIS RS UV-2502 Spectrophotometer was used to determine the concentration of MB at a certain time interval. The wavelength was 664 nm. The absorbance at time t (Q_e) was calculated by Eq(4):

$$Q_e = \frac{(C_0 - C_e).V}{m_0} \tag{4}$$

in which V(L) was the solution volume; C_0 (mg/L) and C_e (mg/L) were the initial and equilibrium concentrations of MB solution, m_0 (g) was the mass of the composite.

The efficiency of MB adsorption was calculated using Eq(5):

$$Efficiency\ (\%) = \frac{(C_0-C_e).100}{C_0} \tag{5}$$

in which, C_0 (mg/L) and C_e (mg/L) were the initial and equilibrium concentrations of MB solution.

2.5.2 Adsorption of oils

The aerogels were coated with MTMS to have a hydrophobic surface following a well-known procedure from previous studies (Nguyen et al., 2013). The capacity of the aerogel with respect to oil adsorption was obtained via the method ASTM F726 - 06 (Nguyen et al., 2013). The two oils were 10W30 motor (viscosity of 244.9 cP at 25 °C) and soybean (viscosity of 5.6 cP at 25 °C) oils. The procedure started with 100 mL oil added into the 250 mL beaker containing the aerogel. After taking the aerogel sample out of the oil beaker, it was dropped quickly on the tissue until a very thin layer remained on the sample surface. This step was performed to remove the excess oil covered outside the aerogel. These two steps were repeated until the measurement values remained unchanged. The amount of oil adsorbed (Q_t) by the aerogel was determined by Eq(6):

$$Q_t = \frac{m_w - m_d}{m_d} \tag{6}$$

in which Q_t (g/g) was the oil adsorption after the time t (second), m_d (g) was the mass of the aerogel before the study, and m_w (g) was the mass of aerogel after the adsorption. The maximum amount of oil adsorbed was determined when the weight of the aerogel after adsorption remained stable.

2.5.3 Adsorption of the heavy metal ion Cu^{2+}

To the 250 mL beaker containing 100 mL of $Cu(NO_3)_2.3H_2O$ was added a certain amount of aerogel. An aliquot (10 mL) of the solution was taken out using pipette and added into a volumetric flask every 10 min. Distilled water was added until obtaining 100 mL solution. The Cu^{2+} adsorption capacity was determined by atomic absorption spectroscopy (AAS) using a Perkin Elmer's AAS atomic spectrometer at the Institute of Environment and Natural Resources, Ho Chi Minh City. In AAS method, the wavelength to measure Cu^{2+} ion was 324.7 nm. The ratio of air to acetylene was 5.6 to 0.6 mL/min. The calculation for Cu^{2+} ion adsorption capacity was identical to oil adsorption.

3. Result and discussion

3.1 Morphology and properties of aerogels

Two types of aerogels were obtained with the same mass ratio of components. The results of BET surface areas and pore sizes were presented in Table 1.

Table 1: Material components (mass ratio) and characterizations

Sample	GO	CNC/Rice straw	PVA	Density (g/cm³)	Porosity (%)	BET surface area (m²/g)	Pore volume (cm³/g)	Pore diameter (nm)
A1	1	30	10	0.0197	98.53	19.718 ± 0.0883	0.088	17.862
A2	1	30	10	0.0385	97.14	13.593 ± 0.2051	0.098	28.716

In Table 1, both aerogels exhibited low density and high porosity. A residue of lignin and hemicellulose in pre-treated rice straw fibre caused an increase of density and a decrease of porosity of A2 in comparison to A1 sample. The results showed that the aerogel from CNC had higher porosity than that obtained from rice straw cellulose. Differences between the dimension of CNC and rice straw fibres led to the smaller overall pore volume of A1 than A2. The morphology and features of aerogels were shown in Figure 1.

Figures 1a and 1b illustrated the SEM images of A1 sample, while Figures 1c and 1d represented that of A2 sample. The specific structure of aerogel was observed easily from these illustrations. GO layer linked to cellulose fibre via hydrogen bonding of PVA chains. In Figure 1a, the sponge-like morphology and bondages were shown in aerogel 3D structural form. Aerogel fabricated from CNC exhibited a homogeneous structure since CNC performed higher disperse ability than rice straw fibre. Thin GO layers covered around CNC and linked with PVA layers. The carbon skeleton frame forming by GO, PVA and CNC created pores inside the aerogel. In Figure 1d, the rice straw fibre, GO sheets and PVA were noticed. The FT-IR analysis of pre-treated rice straw, GO, A2 and A1 samples were presented in Figure 1e.
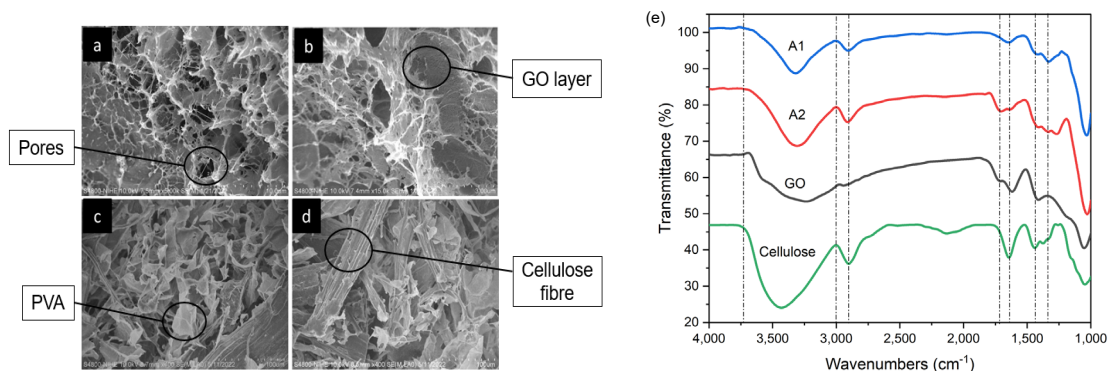
Figure 1: Morphology and properties of aerogels: (a), (b): SEM image of A1; (c), (d): SEM image of A2 and (e) FT-IR spectra of pre-treated rice straw fibre, GO, A1 and A2 samples

The FT-IR analysis of pre-treated rice straw, GO, A2 and A1 samples were presented in Figure 1e. Characteristic peaks of cellulose and GO were noticed. The peak at $3,500 - 3,200$ cm^{-1} corresponded to the valence vibration of the O-H bond. The sharp peak at $2,950$ cm^{-1} corresponded to the covalent vibration of the C-H bond (Nguyen et al., 2022). The sharp absorption tip about $1,000$ cm^{-1} corresponded to the valence oscillation of the C-O bond (Liu et al., 2015). The peaks between $1,600$ and $1,200$ cm^{-1} attributed to the strain vibrations of the C-H bonds (Hossain et al., 2016). The TGA analysis of two samples were shown in Figure 2.
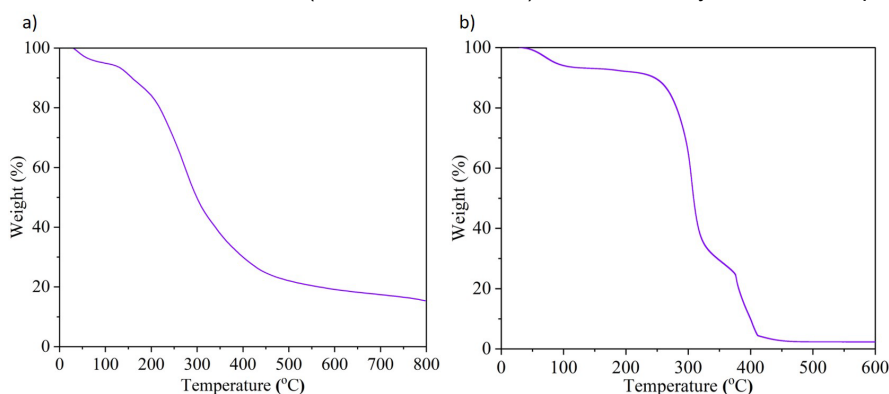

Figure 2. TGA analysis of (a) A1 and (b) A2 aerogels.

Two samples had a common peak at low temperature (150 °C) due to the removal of adsorbed water and solvent residues. In Figure 2a, A1 sample gradually collapsed from 200 °C to 450 °C due to the decomposition of partial GO, partial CNC, and PVA. Above 550 °C, the weight of the aerogel remained nearly constant at 20 %, indicating the CNC presence (D'Acierno et al., 2020). In Figure 2b, A2 sample collapsed from 200 °C to 450 °C due to PVA decomposition (at 200 °C), cellulose and non-cellulose (hemicellulose, lignin) and GO (Nguyen et al., 2022). Above 450 °C, the A2 sample was decomposed completely. It can be seen that A1 sample is not decomposed totally up to 800 °C, while as A2 sample is almost decomposed above 450 °C.

3.2 Adsorption capacity of methylene blue (MB)

MB solutions with different initial concentrations (3 ppm, 4 ppm, 5 ppm) were used to test the adsorption capacity of two aerogels. The MB adsorption results were presented in Table 2.

Table 2: MB adsorption capacity of aerogels

	A1			A2		
Initial concentration C_o (ppm)	3	4	5	3	4	5
q_e, exp (mg/g)	2.859	3.091	3.251	1.911	2.336	2.965
Efficiency (%)	77.83	80.15	66.1	44.91	96.23	36.85

In Table 2, as the initial concentration of MB increased, the adsorption capacity of both aerogels increases. At equilibrium of 4 ppm, A2 adsorbed 96.23% of MB in comparison to 80.15 % of MB in A1. The adsorption kinetics

were investigated following the pseudo-first order and pseudo-second order kinetic model. The results showed that the oil adsorption experiments follow the *pseudo-second-order* kinetic model with the R^2 values close to 1, as shown in Figure 3.
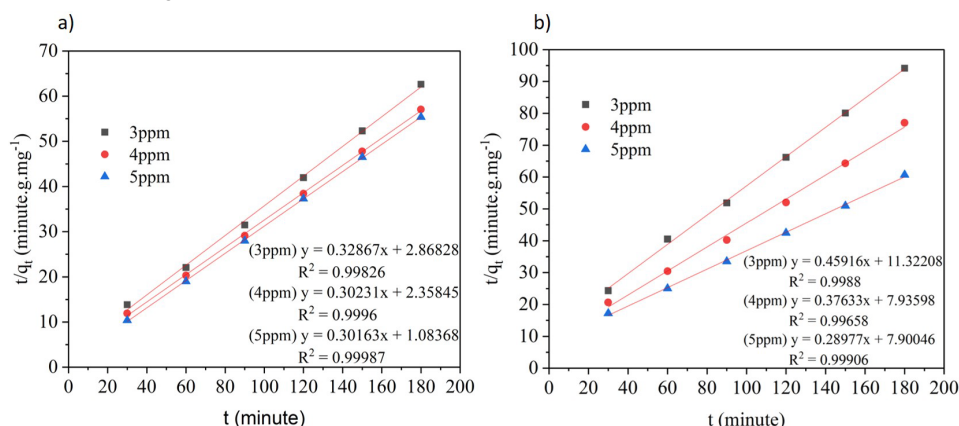

Figure 3: The pseudo-second order kinetic adsorption model of (a) A1 and (b) A2 aerogels.

3.3 Oil adsorption capacity

In this study, 10W30 motor oil and soybean oil were used to test the oil adsorption capability of aerogels. The capacity of oil adsorption was presented in Table 3.

Table 3: Oil adsorption capacity of aerogels

Sample	Motor oil (g/g)	Soybean oil (g/g)	Time reaches equilibrium (s)
A1	21.25	26.18	30
A2	26.66	28.11	30

From Table 3, the aerogels exhibited a high oil adsorption capacity, for both motor oil and soybean oil. Both samples adsorbed soybean oil better than motor oil in a range of 10 % to 20 %. The suitable reason could be due to the lower viscosity of soybean oil compared to that of motor oil. A2 adsorbed oil better than A1 aerogel did. It was noticed that the equilibria of adsorption time reached rapidly within 30 s. Experimentally, both oil adsorption processes followed second-order kinetic model, as shown in Figure 4a and 4b.
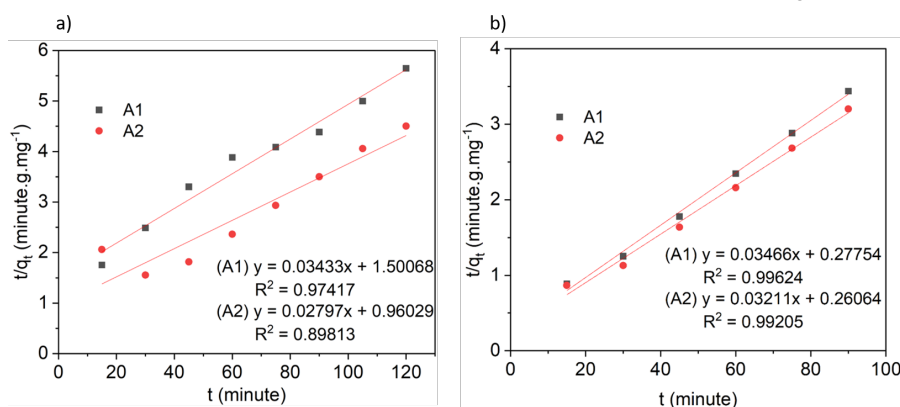

Figure 4: The pseudo-second order kinetic oil adsorption model of (a) motor oil and (b) soybean oil

3.4 Cu²⁺ adsorption capacity

The Cu^{2+} adsorption capacity are shown in Table 4. The aerogels possessed high Cu^{2+} adsorption ability. This could be due to the electrostatic interaction between GO surface (negative charge) and Cu^{2+} (positive charge). The Cu^{2+} adsorption capacity of A1 (123.2 mg/g) was higher than A2 (98.73 mg/g) because of higher porosity of A1 aerogel. A1 showed best adsorption performance: approximately 1.2 times higher than that of cellulose nanofibril (103.5 mg/g) (Tang et al., 2019a) and 2.7 times higher than that of cellulose-graphene oxide carbon aerogel (45.5 mg/g) (Tang et al., 2019b).

Table 4: Cu^{2+} adsorption capacity of aerogel samples

Sample	C$_e$ (mg/l)	q$_{max}$ (mg/g)
A1	53.5	123.2
A2	56.2	98.73

4. Conclusion

A facile fabrication has been developed to obtain a promising candidate for wastewater treatment from agricultural by-products. The aerogels have been well characterized using FT-IR, TGA, nitrogen physisorption isotherm and SEM techniques. The samples possessed light density (about 0.02-0.04 g/cm^3), high porosity (97-98.5 %), high Cu^{2+} and oil absorption capacity and the capability to adsorb cationic dye like MB (efficiency ranged from 80-97% with appropriate concentration). The kinetic studies revealed that the adsorption of methylene blue and oil follows second-order kinetic models since the R^2 value nearly reached 1. The green process can be applied to various source of biomass to create a novel material to solve environmental problems.

Acknowledgments

References

D'Acierno F., Hamad Y.W., Michal C.A., Maclachlan J.M., 2020, Thermal Degradation of Cellulose Filaments and Nanocrystals, Biomacromolecules, 21, 8, 3374-3386.

Hossain I., Anjum N., Tasnim T., 2016, Removal of Arsenic from Contaminated Water Utilizing Tea Waste, International Journal of Environmental Science and Technology, 13, 843-848.

Jiang W., Yao C., Chen W., Li D., Zhong L., Liu C., 2020, A Super-Resilient and Highly Sensitive Graphene Oxide/Cellulose-Derived Carbon Aerogel, Journal of Materials Chemistry A, 8(35), 18376-18384.

Liu L., Gao Z.Y., Su X.P., Chen X., Jiang L., Yao J.M., 2015, Adsorption Removal of Dyes from Single and Binary Solutions Using a Cellulose-Based Bio-Adsorbent, ACS Sustainable Chemistry and Engineering, 3, 432-442.

Long L.Y., Weng Y.X., Wang Y.Z., 2018, Cellulose Aerogels: Synthesis, Applications, and Prospects, Polymers, 10, 623.

Low J.H., Andenan N., Rahman W.W.A., Rusman R., Majid R.A., 2017, Evaluation of Rice Straw as Natural Filler for Injection Molded High Density Polyethylene Bio-Composite Materials, Chemical Engineering Transactions, 56, 1081-1086.

Morimoto N., Kubo T., Nishina Y., 2016, Tailoring the Oxygen Content of Graphite and Reduced Graphene Oxide for Specific Applications, Scientific Reports, 6, 21715.

Nguyen S.T., Feng J., Le N.T., Le A.T.T., Hoang N., Tan V.B.C., Duong H.M., 2013, Cellulose Aerogel from Paper Waste for Crude Oil Spill Cleaning, Industrial & Engineering Chemistry Research, 52, 18386-18391.

Nguyen V.T., Ha L.Q., Nguyen T.D.L., Ly P.H., Nguyen D.M., Hoang D.Q., 2022, Nanocellulose and Graphene Oxide Aerogels for Adsorption and Removal Methylene Blue from An Aqueous Environment, ACS Omega, 7(1), 1003-1013.

Tang J., Song Y., Zhao F., Spinney S., Bernades J.S., Tam K.C., 2019a, Compressible Cellulose Nanofibril (CNF) Based Aerogels Produced Via a Bio-Inspired Strategy for Heavy Metal Ion and Dye Removal, Carbohydrate Polymers, 208, 404-412.

Tang L., Feng Y., He W., Yang F., 2019b, Combination of Graphene Oxide with Flax-Derived Cellulose Dissolved in NaOH/Urea Medium to Generate Hierarchically Structured Composite Carbon Aerogels, Industrial Crops and Products, 130, 179-183.

Wan C., Li J., 2016, Graphene Oxide/Cellulose Aerogels Nanocomposite: Preparation, Pyrolysis, and Application for Electromagnetic Interference Shielding, Carbohydrate Polymers, 150, 172-179.

Wang Z., Song L., Wang Y., Zhang X.F., Yao J., 2021, Construction of A Hybrid Graphene Oxide/Nanofibrillated Cellulose Aerogel Used for The Efficient Removal of Methylene Blue and Tetracycline, Journal of Physics and Chemistry of Solids, 150, 109839.

Wei X., Huang T., Yang J.H., Zhang N., Wang Y., Zhou Z.W., 2017, Green Synthesis of Hybrid Graphene Oxide/Microcrystalline Cellulose Aerogels and Their Use as Superabsorbents, Journal of Hazardous Materials, 335, 28-38.

Zhang J., Cao Y., Feng J., Wu P., 2012, Graphene-Oxide-Sheet-Induced Gelation of Cellulose and Promoted Mechanical Properties of Composite Aerogels, The Journal of Physical Chemistry C, 116(114), 8063-8068.